Characterization of Arctic Sea Ice using L, S and X-Band Fully Polarimetric Airborne F-SAR System

Suman Singha, Remote Sensing Technology Institute (IMF), German Aerospace Center (DLR), Henrich Focke Str. 4 28199 Bremen Germany, Suman.Singha@dlr.de
Marc Jäger, Microwaves and Radar Institute (HR), German Aerospace Center (DLR), Münchener Str. 20, 82230 Weßling, Germany, Marc.Jaeger@dlr.de,

Abstract

Sea ice monitoring has attracted increasing attention over the last few decades. Besides the scientific interest in sea ice, the operational aspect of ice charting is becoming more important due to growing navigational possibilities in an increasingly ice free Arctic. Despite proven sea ice classification achievements on single polarimetric SAR data, a fully automated, general purpose classifier for single-pol data has not been established due to large variation of sea ice manifestations and incidence angle impact. Recently, through the advent of polarimetric SAR sensors, polarimetric features have moved into the focus of ice classification research. The higher information content four polarimetric channels promises to offer greater insight into sea ice scattering mechanism and overcome some of the shortcomings of single-polarimetric SAR for sea ice type discrimination. In this study, fully polarimetric data in L, S and X-band simultaneously acquired by DLR's FSAR system are investigated. Specific dataset were acquired in the framework of DLR-DALO ARCTIC'15 campaign over west Greenland. Proposed supervised classification algorithm consists of two steps: The first step comprises a feature extraction, the results of which are ingested into a neural network classifier in the second step for training and validation. Based on the common coherency and covariance matrix, we extract a number of features and analyze the relevance and redundancy by means of mutual information for the purpose of sea ice classification. Usefulness of different polarimetric features at different frequency bands will be investigated using mutual information analysis along with quantitative comparison of classification results at different frequency bands. Validation of sea ice classification results with Across Track Interferometry (XTI) - derived freeboard measurement is ongoing and initial results are reported.

1 Introduction

Most research published so far on SAR based sea ice classification concentrates on single polarized data at one frequency band (e.g. [2, 10, 17, 4, 13, 9]). Such work naturally concentrates on classical image analysis tools. Among such tools are texture analysis via gray level co-occurrence matrices (GLCM), (cf. [8, 17, 2]), autocorrelation methods([7]) and Markov random fields (MRF)([10]). However useful and successful these techniques may be, there are still major obstacles in sea ice classification, that remain for all mentioned approaches. Most prominent is the high variability of different ice types by influence of incidence angle, weather conditions, location and season.

Multi frequency Fully polarimetric observations from state of the art airborne SAR sensors promises to cope better with these obstacles, since each acquisition contains more information than only one SAR channel [6]. The different backscatter behaviors in different microvave frequencies and polarization channels allow for a better characterization of different ice types. The first known multi-frequency fully polarimetric airborne SAR (AIRSAR, Jet Propulsion Laboratory) acquisition over sea ice was carried out in 1988 and observations were reported in [6]. Where authors reported that such a multi frequency fully polarimetric SAR system is an invaluable tool specially contributions from lower frequency bands in order to extract sea ice geophysical information.

2 Dataset and Methodology

The Airborne SAR imagery used in this study were acquired by German Aerospace Center's (DLR) F-SAR system. The DLR-DALO-ARCTIC flight campaign of 2015 took place in April and May. The campaign was jointly organized by the Danish Defence Acquisition and Logistics Organization (DALO) and the German Aerospace Center (DLR). The principal goals of the campaign were twofold: To analyze the potential of high-resolution polarimetric SAR for security and environmental protection applications in Arctic environments on the one hand, and on the other hand to investigate various advanced methods for extracting ice and snow parameters from SAR data. F-SAR's main design feature is the fully polarimetric operation in five frequency bands, X-, C-, S-, L- and P- band, with the abil-

ity to measure several different frequency bands and/or polarizations simultaneously [12]. It also features high radiometric accuracy and spatial resolution as well as across-track interferometers in X- and S-band. The particular dataset were acquired simultaneously in L, S and X band (fully-polarimetric) on 22nd of May 2015 at 16:57 UTC (approx.) over west of Greenland (above Arctic Circle, see Fig. 1). Two data acquisition have been carried out (PS02 and PS03) in repeat pass interferometric mode (PS02 and PS03 are both in right looking Configuration) covering 102 km in azimuth and 4 km in range direction for each data takes. Fully polarimetric acquisitions in L, S and X band have been used for classification purpose and sea ice freeboard measurements derived from X-band single pass interferometric mode acquisitions have been utilized here to assess the accuracy of the proposed classifier.

During the DALO-ARCTIC F-SAR campaign to Greenland in 2015 [11], multi-spectral polarimetric SAR imaging was employed on most of the test-sites. During the campaign datasets were acquired in one of three configurations: XCL-, XSL- and P-Band, where XSL and XCL could be toggled from pass to pass (i.e. within minutes). During this particular acquisition used in this study XSL combination was selected.

Ice conditions comprised a mixture of Young Ice (YI), Smooth First Year Ice (SFYI) and Rough First/Multi Year Ice (RFMYI) along with small patches of Open Water (OW) between SFYI and RFMYI floes. As training dataset we chose small image patches from PS03 acquisitions representing each of the dominant ice types (indicated by rectangles in Fig. 1 with corresponding ice type color, *i.e.* Blue - Open Water/Nilas (OW), Purple - Young Ice (YI), Yellow - Smooth First Year Ice (SFYI), Red - Rough First Year/Multi Year Ice (RFYMYI)). The variation in backscatter behavior of the four acquisitions differ due to different frequency bands or incidence angle range. Training data rectangles in the image were determined by visual judgment (e.g. using Pauli RGB representation, Co Pol Power Ratio) in conjunction with archive data (Official ice charts and local temperature) of ice situation for the location and time of the year. Ice concentration charts of the Danish Meteorological Institute (DMI) reported a local average sea ice concentration of 90%. According to NASA MODIS data on 2015/05/22 (OB.DAAC), the sea surface temperature in the region of datatakes was around -5 ˚ Celsius (apart from open water portions). The regime of dominant ice classes found were Open Water (OW), Young Ice (YI) and mixture of Smooth First/Multi Year Ice (SFMYI) and Rough First/Multi Year Ice (RFYMYI). After selecting the training area we extracted a total of 18 polarimetric features along with their local variances to build a feature space. Details of each polarimetric feature and their mathematical expressions are described in [14, 15]. After extracting the features we train three separate Artificial Neural Networks which are designed to classify FSAR imagery in L, S and X bands. It is important to note here that we selected same training area for different ice types in L, S and X bands.

Table 1: F-SAR's principal imaging parameters. Repeat-pass InSAR modes are available at all bands.SP InSAR : Single Pass Interferometric Mode.

	X	C	S	L	P
Freq. [GHz]	9.6	5.3	3.25	1.325	0.435
PolSAR	quad	quad	quad	quad	quad
SP InSAR	✓	-	✓	-	-
BW [MHz]	760	380	300	150	50
power [W]	2500	1000	1250	750	750
rg res. [m]	0.25	0.5	0.6	1.0	4.0
az res. [m]	0.1	0.25	0.3	0.5	2.0
swath [km]	2 to 5, depending on aircraft altitude				

3 Classification Results

The processing chain was implemented in the Exelis IDL programming language (image ingestion, calibration, feature extraction, statistical analysis) and in C (ANN classifier). The hardware specifications we used were: 14 GB RAM, Intel Core i-7 3740 QM, virtual linux OS. The processing time was 20 min in total for feature extraction and classification. In order to validate the stability of the training process, we randomly split the initial training data patches into two disjoint subsets (training and reference samples). The classification results compared to reference data samples (as presented in Tables 2, 3 and 4) exhibit a very promising accuracy, which underscores the stability of our algorithm. The percentages in the matrix indicate the proportion of samples of one reference class that were assigned to the respective ice type by the classifier. Therefore columns add up to 100%. Fig. 1 shows the classification results obtained in L, S and X band along with Pauli RGB representation.

Table 2: Classification results compared to reference data samples from each class, FSAR acquisition: 22/05/2015 PS03 T12x4 **L band**

.

	Reference ice class			
ANN Result	OW	YI	SFYI	RFMYI
OW	100.0%	0%	0%	0%
YI	0%	97.6%	0.6%	0%
SFYI	0%	2.0%	99.4%	0.5%
RFMYI	0 %	0.4%	0%	99.5%

Table 3: Classification results compared to reference data samples from each class, FSAR acquisition: 22/05/2015 PS03 T12x4 **S band**

.

	Reference ice class			
ANN Result	OW	YI	SFYI	RFMYI
OW	100.0%	0%	0%	0%
YI	0%	96.9%	0%	0%
SFYI	0%	1.57%	100%	0.8%
RFMYI	0 %	1.53%	0%	99.2%

Table 4: Classification results compared to reference data samples from each class, FSAR acquisition: 22/05/2015 PS03 T12x4 **X band**

	Reference ice class			
ANN Result	OW	YI	SFYI	RFMYI
OW	100.0%	0%	0%	0%
YI	0%	87.60%	3.25%	2.13%
SFYI	0%	8.90%	94.75%	5.42%
RFYMYI	0 %	3.50%	2.0%	92.45%

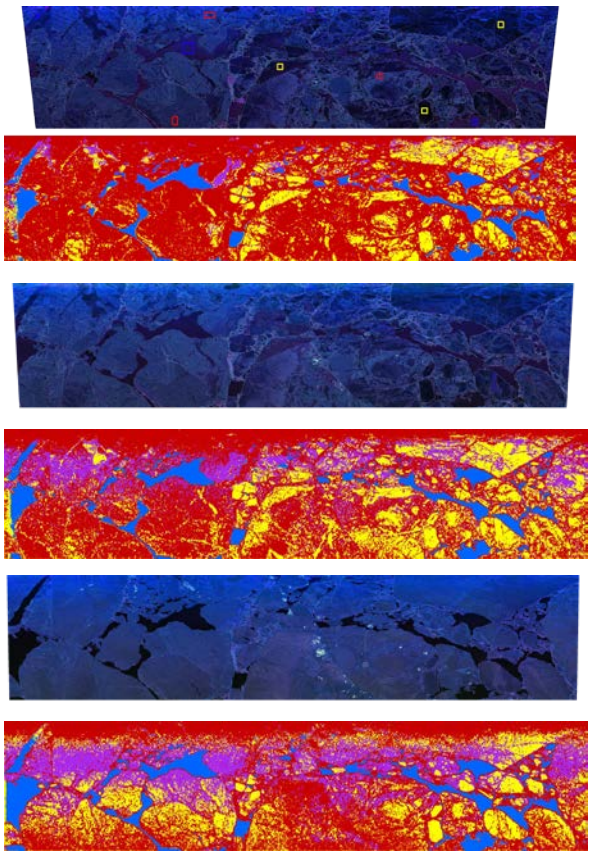

Figure 1: Top to Bottom: (a) Pauli RGB composite of the L-band FSAR acquisition on 2015/05/22, 16:57:49 UTC. (b) L- band Ice classification. (c) Pauli RGB composite of the S-band FSAR acquisition on 2015/05/22, 16:57:49 UTC. (d) S- band Ice classification. (e) Pauli RGB composite of the X-band FSAR acquisition on 2015/05/22, 16:57:49 UTC. (f) X- band Ice classification. Training locations for different classes are shown in Fig (a). **Legend:** Blue - Open Water/Nilas (OW), Purple - Young Ice (YI), Yellow - Smooth First Year Ice (SFYI), Red - Rough First Year/Multi Year Ice (RFYMYI).

Table 2,3 and 4 provide us with an overview of the classifier performance in different frequency bands. In terms of overall classification accuracy L-band perform slightly better than S- and X- band. However when it comes to the differentiation between OW and other ice types, all frequency band performed extremely well. Young Ice (newly formed ice) is to some extend over-represented in X-band most likely due its higher noise floor compared to L-band. We also remark that at the extreme edges (Far Range and Near Range) the performance of the classifier becomes unreliable, specially for higher frequency bands. In Fig. 2 we also compaired the classification results obtained from different frequency bands on pixel by pixel basis. In order to carry out this comparisons, classified images form different frequency bands are first geo-coded and then we identified the pixels where classes differs from each other (i.e. producing a binary layer where 1 represent mismatch). Majority of the mismatches occur on the boundary of different classes (e.g. boundery between OW and SFYI) which are mainly due to different characteristics of sea ice under different frequency band. According to our observation varying penetration depth of different frequency band and presence of snow plays a major role on the performance of the classification scheme.

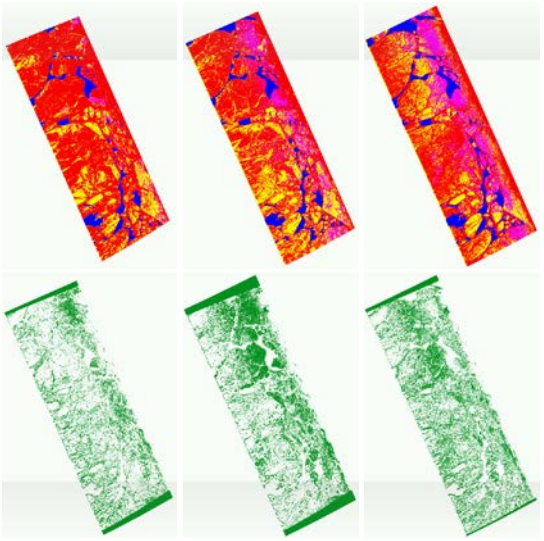

Figure 2: Top(Left to Right): L-, S-, and X- band Ice classification. **Legend:** Blue - Open Water/Nilas (OW), Purple - Young Ice (YI), Yellow - Smooth First Year Ice (SFYI), Red - Rough First Year/Multi Year Ice (RFYMYI).**Top(Left to Right):** Pixel-wise class mis match between L- and S-band, L- and X-band, S- and X-band,

The classified sea ice types are here compared to the high resolution interferometric measurements, e.g. single pass accross track (XTI) derived freeboard. This kind of comparisons of SAR based sea ice classification results, with comparable resolution to SAR acquisitions, are rare due to the challenging nature of the Arctic environment and high associated costs for air-

borne measurements.

To relate the XTI freeboard measurements to the sea ice thickness (T), [3] and[16] found that the freeboard values (h_f) should be multiplied with a factor k. Where k depends on the sea ice, snow and water density and the sea ice and snow height.

$$T = k \times h_f \tag{1}$$

A more detailed study by [5], found that for young ice the k-value is 1-2, for level ice is equal to 4.4, for deformed ice is equal to 5.2. It is important to mention here that those studies are based on Laser-based freeboard measurement which have slightly different properties than SAR XTI based freeboard measurements, mainly due to the penetration capabilities of microwave signal and SAR interferometric imaging mechanism. As the XTI freeboard measurements are derived from X-band and it is well known that the penetration capabilities of this specific frequency band is very limited, specially in the absence of dry snow cover. Manually selected ROIs were used to extract XTI freeboard values from the different sea ice types (classified) and the open water within the X-band scenes. The relationship between the sea ice types and theoretical sea ice freeboards are given in Table 5, together with observed sea ice freeboard derived from XTI measurements. It is observed that the selected sections of classified images (*i.e.* classified ice types) show good agreement with observed XTI derived freeboard, and in accordance with the WMO standard for sea ice types [1].

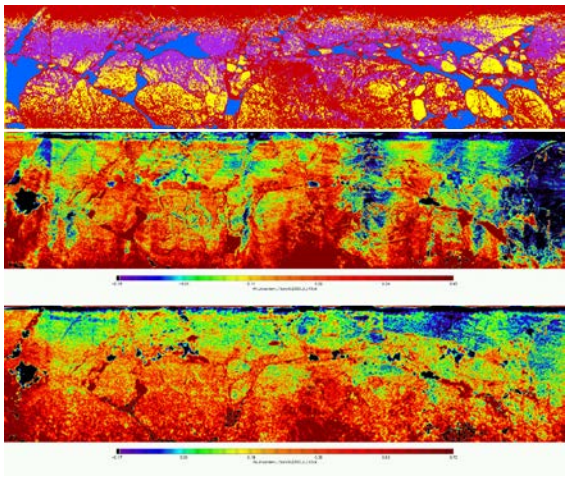

Figure 3: Top: X- band Ice classification. Blue - Open Water/Nilas (OW), Purple - Young Ice (YI), Yellow - Smooth First Year Ice (SFYI), Red - Rough First Year/Multi Year Ice (RFYMYI) **Middle:**XTI (HH channel) derived freeboard measurements in meter. **Bottom:**XTI (HV channel) derived freeboard measurements in meter

Table 5: Estimated sea ice freeboards for the different sea ice types as well as observed XTI (HH) sea ice freeboard. The sea ice thickness is given according to WMO Sea Ice Nomenclature.

Sea Ice Type	Sea Ice Thickness	Estimated Sea Ice Freeboard	Observed XTI Freeboard (HH)
OW	<0.1 m	<0.05 m	0.00 m ± 0.05 m
YI	0.1 m-0.3 m	0.05 m-0.15 m	0.08 m ± 0.06 m
SFYI	0.3 m-2.0 m	0.07 m-0.45 m	0.15 m ± 0.15 m
RFYMYI	> 2 m	>0.36 m	0.27 m ± 0.18 m

4 Conclusions

Until recently sea ice classification using airborne SAR was rather uncharted research domain. We investigated the potential of DLR's FSAR fully polarimetric data for automated sea ice classification in L, S and X-band. We deem the distinction of all classes in different frequency bands are quite promising. Remarking that both training and validation data are from the same ice situation (*i.e.*, same time, location and incidence angle), our method displays consistency in itself and stability with respect to the choice of training data in different frequency bands. Validation of the classification results with freeboard measurements derived form XTI measurement is ongoing. A detailed statistical analysis of different polarimetric features with respect to class separation and a quantitative analysis of classification results in different frequency bands will be included in the final manuscript. Future work on improvement of the classification technique will include identification of optimum polarimetric features and reduction of feature space which will facilitate shorter processing time.

5 Acknowledgment

FSAR dataset were acquired in the framework of DLR-DALO ARCTIC'15 Campaign. Authors would like to thank the campaign team for their immense effort.

References

[1] Wmo sea-ice nomenclature: Wmo/td-no. 259. [2]

D.A. Clausi and Bing Yue. Comparing cooccurrence probabilities and Markov random fields for texture analysis of SAR sea ice imagery. *Geoscience and Remote Sensing, IEEE Transactions on*, 42(1):215–228, Jan 2004.

[3] J. C. Comiso, P. Wadhams, W. B. Krabill, R. N. Swift, J. P. Crawford, and W. B. Tucker. Top/bottom multisensor remote sensing of arctic sea ice. *Journal of Geophysical Research: Oceans*, 96(C2):2693–2709, 1991.

[4] Wolfgang Dierking and Leif Toudal Pedersen. Monitoring sea ice using ENVISAT ASAR - a new era starting 10 years ago. In *IEEE International Geoscience and Remote Sensing Symposium 2012*, on CD ROM, July 2012. IEEE.

[5] Martin J. Doble, Henriette Skourup, Peter Wadhams, and Cathleen A. Geiger. The relation between arctic sea ice surface elevation and draft: A case study using coincident auv sonar and airborne scanning laser. *Journal of Geophysical Research: Oceans*, 116(C8):n/a–n/a, 2011. C00E03.

[6] Mark R. Drinkwater, R. Kwok, D. P. Winebrenner, and E. Rignot. Multifrequency polarimetric synthetic aperture radar observations of sea ice. *Journal of Geophysical Research: Oceans*, 96(C11):20679–20698, 1991.

[7] J. Karvonen, M. Simila, and M. Makynen. Open Water Detection From Baltic Sea Ice Radarsat-1 SAR Imagery. *IEEE Geoscience and Remote Sensing Letters*, 2:275–279, July 2005.

[8] Ronald Kwok, Eric Rignot, Benjamin Holt, and R. Onstott. Identification of sea ice types in spaceborne synthetic aperture radar data. *Journal of Geophysical Research: Oceans*, 97(C2):2391–2402, 1992.

[9] S. Leigh, Zhijie Wang, and D.A. Clausi. Automated Ice-Water Classification Using Dual Polarization SAR Satellite Imagery. *Geoscience and Remote Sensing, IEEE Transactions on*, 52(9):5529–5539, Sept 2014.

[10] S. Ochilov and D.A. Clausi. Operational SAR Sea-Ice Image Classification. *Geoscience and Remote Sensing, IEEE Transactions on*, 50(11):4397–4408, Nov 2012.

[11] A. Reigber, E. Krogager, M. Keller, M. Jaeger, I. Hajnsek, and R. Horn. The dalo-arctic campaign: Multi-spectral sar imaging of ice features in greenland. In *Proceedings of EUSAR 2016: 11th European Conference on Synthetic Aperture Radar*, pages 1–3, June 2016.

[12] A. Reigber, R. Scheiber, M. Jager, P. Prats-Iraola, I. Hajnsek, T. Jagdhuber, K. P. Papathanassiou, M. Nannini, E. Aguilera, S. Baumgartner, R. Horn, A. Nottensteiner, and A. Moreira. Very-high-resolution airborne synthetic aperture radar imaging: Signal processing and applications. *Proceedings of the IEEE*, 101(3):759–783, March 2013.

[13] R. Ressel, A. Frost, and S. Lehner. A neural network-based classification for sea ice types on x-band sar images. *IEEE Journal of Selected Topics in Applied Earth Observations and Remote Sensing*, 8(7):3672–3680, July 2015.

[14] Rudolf Ressel and Suman Singha. Comparing near coincident space borne c and x band fully polarimetric sar data for arctic sea ice classification. *Remote Sensing*, 8(1):57, 2016.

[15] Suman Singha, A. Malin Johansson, Nicholas Hughes, Sine M. Hvidegaard, and Henriette Skourup. Arctic sea ice characterization using spaceborne fully polarimetric l-, c- and x-band sar with validation by airborne measurements. *IEEE Transaction on Geoscience and Remote Sensing*, -(-):in press, 2018.

[16] P. Wadhams, W. B. Tucker, W. B. Krabill, R. N. Swift, J. C. Comiso, and N. R. Davis. Relationship between sea ice freeboard and draft in the arctic basin, and implications for ice thickness monitoring. *Journal of Geophysical Research: Oceans*, 97(C12):20325–20334, 1992.

[17] N. Y. Zakhvatkina, Vitaly Alexandrov, Ola M. Johannessen, Stein Sandven, and I. Frolov. Classification of sea ice types in ENVISAT synthetic aperture radar images. *IEEE Transactions on Geoscience and Remote Sensing*, 51:2587–2600, 2013.